

---

# Modeling Irregular Time Series with Continuous Recurrent Units

---

Mona Schirmer<sup>1</sup> Mazin Eltayeb<sup>2</sup> Stefan Lessmann<sup>3</sup> Maja Rudolph<sup>4</sup>

## Abstract

Recurrent neural networks (RNNs) like long short-term memory networks (LSTMs) and gated recurrent units (GRUs) are a popular choice for modeling sequential data. Their gating mechanism permits weighting previous history encoded in a hidden state with new information from incoming observations. In many applications, such as medical records, observations times are irregular and carry important information. However, LSTMs and GRUs assume constant time intervals between observations. To address this challenge, we propose continuous recurrent units (CRUs) - a neural architecture that can naturally handle irregular time intervals between observations. The gating mechanism of the CRU employs the continuous formulation of a Kalman filter and alternates between (1) continuous latent state propagation according to a linear stochastic differential equation (SDE) and (2) latent state updates whenever a new observation comes in. In an empirical study, we show that the CRU can better interpolate irregular time series than neural ordinary differential equation (neural ODE)-based models. We also show that our model can infer dynamics from images and that the Kalman gain efficiently singles out candidates for valuable state updates from noisy observations.

## 1. Introduction

Recurrent architectures, such as the long short-term memory network (LSTM) (Hochreiter & Schmidhuber, 1997) or gated recurrent unit (GRU) (Cho et al., 2014b) have become a staple machine learning tool for modeling time series data. Their modeling power comes from a hidden state which is recursively updated to integrate new observations and a gating mechanism to balance the importance of new

information with the history already encoded in the latent state.

Recurrent neural networks (RNNs) typically assume regular sampling rates. However, many real world data sets, such as electronic health records or climate data are irregularly sampled. In irregularly sampled time series data, the time intervals between observations can vary in length. In health care for instance, measurements of a patients health status are only available when the patients goes to the doctor. The time passed between observations also carries information about the underlying time series. A lab test not administered for many months could mean that the patient was doing well in the meantime, while frequent visits might indicate that the patient’s health is deteriorating. Standard RNNs have difficulty modeling such data as they do not reflect the continuity of the underlying temporal processes.

Recently, the work on neural ordinary differential equations (neural ODEs) (Chen et al., 2018) has established an elegant way of modelling irregularly sampled time series. Recurrent ordinary differential equation (ODE)-based architectures determine the hidden state between observations by an ODE and update its hidden state at observation times using standard RNN gating mechanisms (Rubanova et al. 2019; Brouwer et al. 2019; Lechner & Hasani 2020). These methods rely on some form of ODE-solver, a network component that prolongs training time significantly (Rubanova et al. 2019; Shukla & Marlin 2020).

In both standard and ODE-based RNNs, the hidden state is designed as a deterministic component opposed to a random variable. A probabilistic state space however, benefits from theoretical grounds for optimal solutions and allows tracking uncertainty concisely over the transformation steps of observations. Reliable uncertainty quantification is indispensable in decision making contexts such as autonomous driving or AI-based medicine.

We propose continuous recurrent unit (CRU), a probabilistic recurrent architecture for modelling irregularly sampled time series. An encoder maps observations into a latent space. In this latent space, the latent state of the CRU is governed by a linear stochastic differential equation (SDE). The analytic solution for propagating the latent state between observations and the update equations for integrating new observations are given by the continuous-discrete formula-

---

<sup>1</sup>Humboldt-Universität zu Berlin, work done as an intern at the Bosch Center for AI <sup>2</sup>Bosch Center for AI, Germany <sup>3</sup>Humboldt-Universität zu Berlin <sup>4</sup>Bosch Center for AI, USA. Correspondence to: Mona Schirmer <mona.schirmer@freenet.de>, Maja Rudolph <maja.rudolph@us.bosch.com>.

tion of the Kalman filter (Kalman, 1960). Employing the linear SDE state space model and the Kalman filter has three major advantages. First, a probabilistic state space provides an explicit notion of uncertainty for both an uncertainty-driven gating mechanism and for confidence evaluation of predictions. Second, the gating mechanism is optimal in a locally linear state space. Third, the latent state at any point in time can be resolved analytically, therefore bypassing the need for numerical integration techniques. Our contributions are as follows:

- We present the CRU, a time-series model that combines the power of neural networks for feature extraction with the advantages of a probabilistic state-space model, specifically the continuous-discrete Kalman filter (Section 3.1).
- The resulting neural architecture can process time-series data like a recurrent neural network by sequentially processing observations and internally updating its latent states. Due to the properties of the continuous-discrete Kalman filter, the model deals with irregular time intervals between observations in a principled manner.
- An efficient parameterization of the latent state transition via the transition’s eigenspace (Section 3.3) allows us to reduce the model’s complexity significantly and to trade off speed with accuracy.
- In an empirical study (Section 4) we compare the performance of CRU to discrete and continuous baselines on images, electronic health records and climate data. We find that (i) the gating mechanism leverages uncertainty arising from both noisy and partially observed inputs (ii) CRU outperforms discrete RNN counterparts on synthetic image data (iii) our method can better interpolate irregular time series than neural ODE-based methods.

## 2. Related Work

**Deep (probabilistic) sequence models** Classical deep recurrent time series models such as GRU (Cho et al., 2014b) and LSTM (Hochreiter & Schmidhuber, 1997) distill information from incoming data and preserve relevant information in the cell state over a long time horizon. However, it has been argued that a lack of randomness in the internal transitions of such models fail to capture the variability of certain data types (Chung et al. 2015). Probabilistic alternatives infer relevant information in a latent variable model. Recent work has integrated the discrete Kalman filter as probabilistic component into deep learning frameworks (Krishnan et al. 2015; Karl et al. 2016; Fraccaro et al. 2017; Becker et al. 2019). Our method builds up on the idea of Recurrent Kalman networks (RKNs) (Becker et al., 2019).

**RNNs for irregular time series** Applying standard RNNs on irregularly sampled time series necessarily precedes the discretization of the time line into equally spaced bins. However, this typically reduces the number of observation times, results in a loss of information and evokes the need for imputation and aggregation strategies. Approaches to circumvent prior preprocessing propose to augment the observations with timestamps (Choi et al. 2018; Mozer et al. 2017) or observation masks (Lipton et al., 2016). However, such approaches do not grasp the dynamics of the hidden state between observations. In Che et al. (2018) and Cao et al. (2018) the hidden state decays exponentially between observations according to a trainable decay parameter. The idea is to mirror increasing irrelevance of encoded history after much time has passed, which is an assumption that can be inappropriate in some use cases.

**Neural ODEs** Neural ODE-based methods explicitly model the dynamics of the hidden state by an ODE. Chen et al. (2018) proposes latent ODE, a generative model whose latent state evolves according to a Neural ODE. However, there is no update mechanism employed making it impossible to incorporate observations into the latent trajectory that arrive later. Kidger et al. (2020) and Morrill et al. (2021) extended neural ODE with concepts from rough analysis which allows for online learning. ODE-RNN (Rubanova et al., 2019) and ODE-LSTM (Lechner & Hasani, 2020) use standard RNN gates to sequentially update the hidden state at observation times. Both GRU-ODE-Bayes (Brouwer et al., 2019) and Neural Jump ODE (NJ-ODE) (Herrera et al., 2020) enforce a Bayesian update by tightly coupling ODE dynamics and update step via their objective function. As Herrera et al. (2020) point out, there is no theoretical ground that GRU-ODE-Bayes nor ODE-RNN yield optimal predictions. They prove convergence of their NJ-ODE model to the optimal prediction under Markovian assumptions. Let’s note that their framework does not model uncertainty in the gating mechanism.

## 3. Method

The CRU addresses the challenge of modeling a time series  $\mathbf{x}_{\mathcal{T}} = [\mathbf{x}_t | t \in \mathcal{T} = \{t_0, t_1, \dots, t_N\}]$  whose observation times  $\mathcal{T} = \{t_0, t_1, \dots, t_N\}$  can occur at irregular intervals. Figure 1 illustrates the network architecture. An encoder  $f_{\theta}$  and a decoder  $g_{\phi}$  relate observation space with a latent observation and latent state space. CRU assumes Gaussian latent observations  $\mathbf{y}_t$  and a continuous latent state  $\mathbf{z}$  whose dynamics are governed by a linear SDE. In latent space, we alternate between inferring the latent state posterior at observation times and propagating the latent state between observations continuously in time.

At each time point  $t \in \mathcal{T}$ , an observation is propagated

through four internal network steps: A neural network encoder  $f_\theta$  maps the observation  $\mathbf{x}_t$  to a latent observation space and outputs a transformed latent observation  $\mathbf{y}_t$  along with an elementwise latent observation noise  $\sigma_t^{\text{obs}}$ .

$$\text{encoder: } [\mathbf{y}_t, \sigma_t^{\text{obs}}] = f_\theta(\mathbf{x}_t). \quad (1)$$

The posterior computation updates the latent state with the latent observation

$$p(\mathbf{z}_t | \mathbf{y}_t) = \mathcal{N}(\boldsymbol{\mu}_t^+, \boldsymbol{\Sigma}_t^+). \quad (2)$$

Between observations, the latent state prior evolves according to the linear SDE

$$d\mathbf{z} = \mathbf{A}\mathbf{z}dt + \mathbf{G}d\boldsymbol{\beta}, \quad (3)$$

where  $\mathbf{A} \in \mathbb{R}^{M \times M}$  is a time-invariant transition matrix,  $\boldsymbol{\beta} \in \mathbb{R}^B$  a Brownian motion process with diffusion matrix  $\mathbf{Q} \in \mathbb{R}^{B \times B}$  and diffusion coefficient  $\mathbf{G} \in \mathbb{R}^{M \times B}$ .

The decoder maps the posterior estimate to the desired output space along with an elementwise uncertainty estimate.

$$\text{decoder: } [\mathbf{o}_t, \sigma_t^{\text{out}}] = g_\phi(\boldsymbol{\mu}_t^+, \boldsymbol{\Sigma}_t^+). \quad (4)$$

The optimal solution for the latent state inference problem is given by the continuous-discrete Kalman filter. We first describe the continuous-discrete Kalman filter in the next section. Then we introduce design choices for CRU to ensure flexible yet fast state propagation.

### 3.1. Continuous-discrete Kalman filter

The continuous-discrete Kalman filter, see [Jazwinski \(1970\)](#), is the optimal state estimator for a continuous state space model with a discrete-time Gaussian observation process. The latent state  $\mathbf{z} \in \mathbb{R}^M$  is assumed to evolve continuously according to the linear SDE in Equation (3) At times  $t \in \mathcal{T}$  an observation  $\mathbf{y}_t \in \mathbb{R}^D$  is sampled from

$$\mathbf{y}_t \sim \mathcal{N}(\mathbf{H}\mathbf{z}_t, \boldsymbol{\Sigma}_t^{\text{obs}}), \quad (5)$$

where  $\mathbf{H} \in \mathbb{R}^{D \times M}$  denotes the observation model. The noise components of  $\mathbf{y}_t$ ,  $\mathbf{z}_t$  and the initial state  $\mathbf{z}_{t_0}$  are assumed to be independent. This version of the Kalman filter allows modelling discrete observations at potentially arbitrary time-intervals as samples from a continuous trajectory of  $\mathbf{z}$ . Posterior estimates of the latent state can be obtained by Bayes' theorem in a recurrent two-step procedure.

#### 3.1.1. PREDICTION STEP

Between observations the prior density describes the evolution of the latent state. It is governed by the SDE in (3). For linear, time-invariant systems - as it is the case here - the SDE has an analytical solution. After an observation at time

$t$  the solution of the SDE for  $t' > t$  is given by

$$\mathbf{z}_{t'} = \exp(\mathbf{A}(t' - t))\mathbf{z}_t + \int_t^{t'} \exp(\mathbf{A}(t' - \tau))\mathbf{G}d\boldsymbol{\beta}_\tau \quad (6)$$

From here, the prior density at time  $t'$  is  $p(\mathbf{z}_{t'} | \mathbf{y}_t) = \mathcal{N}(\boldsymbol{\mu}_{t'}^-, \boldsymbol{\Sigma}_{t'}^-)$  with

$$\boldsymbol{\mu}_{t'}^- = \exp(\mathbf{A}(t' - t))\boldsymbol{\mu}_t^+ \quad (7)$$

$$\begin{aligned} \boldsymbol{\Sigma}_{t'}^- &= \exp(\mathbf{A}(t' - t))\boldsymbol{\Sigma}_t^+ \exp(\mathbf{A}(t' - t))^T \\ &+ \int_t^{t'} \exp(\mathbf{A}(t' - \tau))\mathbf{G}\mathbf{Q}\mathbf{G}^T \exp(\mathbf{A}(t' - \tau))^T d\tau, \end{aligned} \quad (8)$$

where  $\exp(\cdot)$  denotes the matrix exponential and  $(\boldsymbol{\mu}_t^+, \boldsymbol{\Sigma}_t^+)$  the posterior mean and variance of the latent state at the last observation time  $t$ . Note that the integral in Equation (8) can be resolved analytically using matrix fraction decomposition. Its computation is detailed in Section 6.2. We summarize the prediction step for the parameters of the prior  $p(\mathbf{z}_{t'} | \mathbf{y}_t) = \mathcal{N}(\boldsymbol{\mu}_{t'}^-, \boldsymbol{\Sigma}_{t'}^-)$  as

$$[\boldsymbol{\mu}_{t'}^-, \boldsymbol{\Sigma}_{t'}^-] = \text{predict}(\boldsymbol{\mu}_t^+, \boldsymbol{\Sigma}_t^+, t' - t). \quad (9)$$

#### 3.1.2. UPDATE STEP

At the time of a new observation  $t'$  the prior is updated by Bayes' theorem,

$$p(\mathbf{z}_{t'} | \mathbf{y}_{t'}) = \frac{p(\mathbf{y}_{t'} | \mathbf{z}_{t'})p(\mathbf{z}_{t'} | \mathbf{y}_t)}{p(\mathbf{y}_{t'} | \mathbf{y}_t)}. \quad (10)$$

Thanks to the Gaussian assumption all quantities are known and the posterior density at time  $t \in \mathcal{T}$  is given by  $p(\mathbf{z}_t | \mathbf{y}_t) = \mathcal{N}(\boldsymbol{\mu}_t^+, \boldsymbol{\Sigma}_t^+)$  with

$$\boldsymbol{\mu}_t^+ = \boldsymbol{\mu}_t^- + \mathbf{K}_t(\mathbf{y}_t - \mathbf{H}\boldsymbol{\mu}_t^-) \quad (11)$$

$$\boldsymbol{\Sigma}_t^+ = (\mathbf{I} - \mathbf{K}_t\mathbf{H})\boldsymbol{\Sigma}_t^-. \quad (12)$$

The updates can be seen as weighted averages, where the Kalman gain  $\mathbf{K}_t$  acts as gate between prior and observation. It contrasts observation noise with prior uncertainty and is high when observations are confident.

$$\mathbf{K}_t = \boldsymbol{\Sigma}_t^- \mathbf{H}^T (\mathbf{H}\boldsymbol{\Sigma}_t^- \mathbf{H}^T + \boldsymbol{\Sigma}_t^{\text{obs}})^{-1}. \quad (13)$$

We summarize these updates as

$$[\boldsymbol{\mu}_t^+, \boldsymbol{\Sigma}_t^+] = \text{update}(\boldsymbol{\mu}_t^-, \boldsymbol{\Sigma}_t^-, \mathbf{y}_t, \sigma_t^{\text{obs}}). \quad (14)$$

### 3.2. Locally linear transitions

Similar as in [\(Becker et al., 2019\)](#), we relax the linearity assumption of the Kalman filter to locally linear state transitions. We design the transition matrix  $\mathbf{A}_t$  at time  $t$  as a weighted average of  $K$  parameterized basis matrices. The

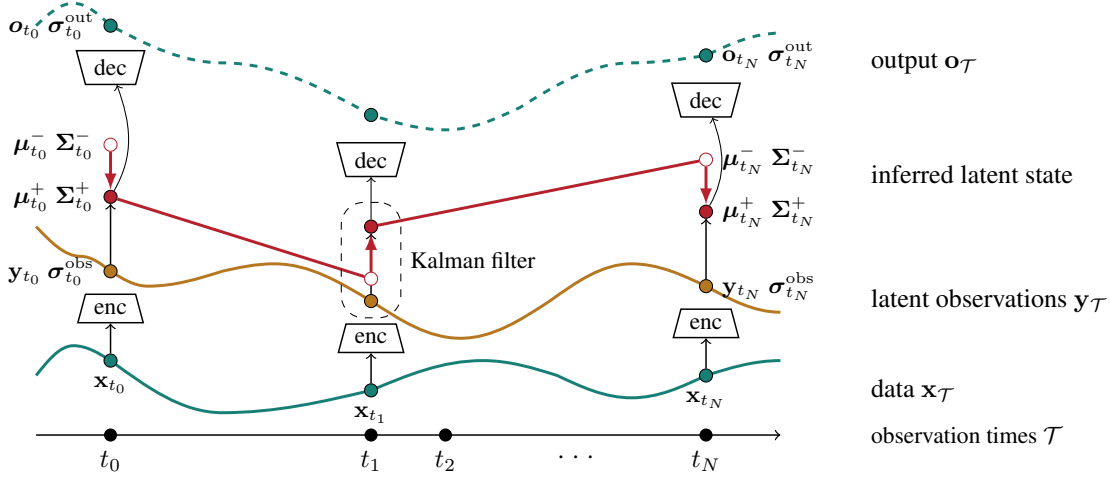


Figure 1. CRU: An encoder network maps the observation  $\mathbf{x}_t$  to a latent observation  $\mathbf{y}_t$  and returns an elementwise uncertainty estimate  $\sigma_t^{\text{obs}}$ . Both are used to update the latent state prior  $\mu_t^-, \Sigma_t^-$  to the latent state posterior  $\mu_t^+, \Sigma_t^+$  (red arrows), which the decoder maps back to the observation space. The latent state posterior is propagated to the next observation time (red lines).

weighting coefficients  $\alpha_t^{(k)}$   $k \in \{1 \dots K\}$  are learned from the current posterior mean  $\mu_t^+$  by a small neural network  $w_\psi$  with softmax output,

$$\mathbf{A}_t = \sum_{k=1}^K \alpha_t^{(k)} \mathbf{A}^{(k)} \quad \text{with} \quad \alpha_t = w_\psi(\mu_t^+). \quad (15)$$

To reduce the number of parameters, each basis matrix consists of four banded matrices with bandwidth  $b$ . In addition, we assume a diagonal diffusion matrix  $\mathbf{Q}$  whose vector of diagonal entries  $\mathbf{q}$  is a time-invariant learnable parameter. The diffusion coefficient  $\mathbf{G}$  of the SDE in Equation (3) is fixed at the identity matrix, i.e.  $\mathbf{G} = \mathbf{I}_{M \times M}$ . The later is insofar not restrictive as  $\mathbf{G}$  only occurs in combination with the learnable parameter vector  $\mathbf{q}$  (Equation (6)), which has maximum flexibility. Algorithm 1 summarizes the network’s internals.

---

#### Algorithm 1 The CRU

---

**Input:** Datapoints and their timestamps  $\{(\mathbf{x}_t, t)\}_{t \in \mathcal{T}}$

**Trainable Parameters:** Encoder, decoder, transition net weights  $\theta, \phi, \psi$ , transition noise  $\mathbf{q}$  and matrices transition matrices  $\{\mathbf{A}_i\}_{i=1 \dots K}$

**Initialize:**  $\mu_{t_0}^-, \Sigma_{t_0}^-$

**for** consecutive timestamps  $(t, t') \in \mathcal{T}, t < t'$  **do**

$\mathbf{y}_t, \sigma_t^{\text{obs}} = f_\theta(\mathbf{x}_t)$

$\mu_t^+, \Sigma_t^+ = \text{update}(\mu_t^-, \Sigma_t^-, \mathbf{y}_t, \sigma_t^{\text{obs}})$

$\mu_{t'}^-, \Sigma_{t'}^- = \text{predict}(\mu_t^+, \Sigma_t^+, t' - t)$

$\mathbf{o}_t, \sigma_t^{\text{out}} = g_\phi(\mu_t^+, \Sigma_t^+)$

**end for**

**Return:**  $\{\mathbf{o}_t, \sigma_t^{\text{out}}\}_{t \in \mathcal{T}}$

---

### 3.3. Efficient Implementation

The runtime of the CRU is dominated by two operations: the matrix inversion in the computation of the Kalman gain (Equation (13)) and the matrix exponential in the prediction step (Equations (7) and (8)). As in Becker et al. (2019), there is a trade-off between modeling flexibility and runtime when choosing how to parametrize the model parameters. Becker et al. (2019) use certain factorization assumptions that increase speed and stability of the computation. CRU also benefits from these assumptions that notably simplify the matrix inversion and are detailed in Section 6.3. Further, we propose an alternative parameterization of the state transitions via the transition’s eigenspace. This approach reduces the costly and numerically unstable matrix exponential of complexity  $O(n^3)$  to matrix multiplication and elementwise operations. This variant exploits assumptions on how far the basis matrices can differ from each other to facilitate computations. It can be seen as a compromise between strictly linear state propagation and locally linear transitions with an unconstrained parameter space.

Precisely, we assume diagonalizable basis matrices  $\{\mathbf{A}^{(k)}\}_{k=1 \dots K}$  that share the same orthogonal eigenvectors. That is to say, for all  $k \in \{1 \dots K\}$  we have  $\mathbf{A}^{(k)} = \mathbf{E} \mathbf{D}^{(k)} \mathbf{E}^T$  where  $\mathbf{D}^{(k)}$  is a diagonal matrix whose  $i$ -th diagonal entry is the eigenvalue of  $\mathbf{A}^{(k)}$  corresponding to the eigenvector in the  $i$ -th column of  $\mathbf{E}$ . When using  $\mathbf{E}$  to perform a change of basis on the latent state  $\mathbf{z}_t$ , the SDE of the transformed state vector  $\mathbf{w}$  has diagonal transitions  $\mathbf{D}$  and its covariance  $\Sigma_{t'}^{\mathbf{w}}$  at time  $t'$  is cheap to resolve. The prior mean at time  $t'$  can be computed by using  $\mathbf{E}$  to project into

the eigenspace,

$$\boldsymbol{\mu}_{t'}^- = \mathbf{E} \exp\left((t' - t) \sum_{k=1}^K \alpha^{(k)} \mathbf{D}^{(k)}\right) \mathbf{E}^T \boldsymbol{\mu}_t^+, \quad (16)$$

where  $\exp(\cdot)$  denotes the elementwise exponential. The prior covariance can be computed efficiently by following the method by Rome (1969). Mapping  $\Sigma_{t'}^w$  back to the original basis of  $\mathbf{z}$  yields the prior covariance at time  $t'$

$$\Sigma_{t'}^- = \mathbf{E} \Sigma_{t'}^w \mathbf{E}^T \quad \text{with} \quad \mathbf{w}_t = \mathbf{E}^T \mathbf{z}_t. \quad (17)$$

We provide the thorough definitions and computations of the alternative prior computation in Section 6.1.2. We refer to this faster variant that picks up the state transitions by learning the eigenvectors  $\mathbf{E}$  and eigenvalues  $\{\mathbf{D}^{(k)}\}_{k=1\dots K}$  as fast continuous recurrent unit (f-CRU).

The above assumptions enclose the space of possible transitions to ones based on commutative, symmetric basis matrices. While this seems restrictive, the free parameters in the encoder and decoder allow for great flexibility to find a suitable state space. In Section 4 we show that the two parameterization options allow for a trade off between speed and accuracy.

### 3.4. Training

The objective function is the Gaussian negative log-likelihood of the ground truth sequence  $\mathbf{s}_{\mathcal{T}}$  and is given for a single sample by

$$\mathcal{L}(\mathbf{s}_{\mathcal{T}}) = -\frac{1}{N} \sum_{t \in \mathcal{T}} \log \mathcal{N}(\mathbf{s}_t | \mathbf{o}_t, (\boldsymbol{\sigma}_t^{\text{out}})^2). \quad (18)$$

When the ground truth  $\mathbf{s}_t$  is binary (e.g. we work with binarized images with  $D_0$  pixels), the model is trained on the Bernoulli negative log-likelihood

$$\mathcal{L}(\mathbf{s}_{\mathcal{T}}) = -\frac{1}{N} \sum_{t \in \mathcal{T}} \sum_{i=1}^{D_0} s_t^{(i)} \log(o_t^{(i)}) + (1 - s_t^{(i)}) \log(1 - o_t^{(i)}). \quad (19)$$

The model parameters  $(\theta, \phi, \psi, \mathbf{q})$  and  $\{\mathbf{A}^{(k)}\}_{k=1\dots K}$  or alternatively  $\mathbf{E}, \{\mathbf{D}^{(k)}\}_{k=1\dots K}$  for f-CRU can be trained with backpropagation in an end-to-end manner. Lezcano-Casado (2019) provides the tools to maintain the orthogonality constraint on  $\mathbf{E}$  during training.

## 4. Empirical Study

We are interested in the performance of CRU on irregularly sampled time series. For that we test the method on data from two typical application domains: meteorology and health care. We compare our method in terms of both predictive power and training time to decay-based RNNs

and neural ODE-based frameworks. We further inspect how the probabilistic state update weights noisy and partially observed input data.

### 4.1. Datasets

**Pendulum Images** We used the pendulum simulation in Becker et al. (2019) to generate 3 000 synthetic image sequences. The 24x24 pixel images show a pendulum at 50 irregular time steps. In the first setting, we remove half of the images per sequence and task the models to impute the missing frames. In the second setting, we keep the entire sequence and add a correlated noise process to the images as in Becker et al. (2019). The noise increases over consecutive time steps resulting in images potentially consisting of pure noise. Here, we evaluate the models on detecting the pendulum angle  $\boldsymbol{\theta}_t = (\sin(\theta_t), \cos(\theta_t))$  at each time step.

**Climatic data** We use data from the United States Historical Climatology Network (USHCN) (Menne et al., 2015). The dataset contains daily measurements from 1218 weather stations across the United States for five variables: precipitation, snowfall, snow depth, minimum and maximum temperature. We select a subset of 1168 meteorological stations over a range of four years from 1990 to 1993. Though collected in regular time intervals, climatic data is often sparse due to e.g. sensor failures. To further increase the sparsity of the data across time and across dimensions we first subsample 50% of the time points and then randomly remove 20% of the measurements.

**Electronic health records** We benchmark the models on the data set of the Physionet Computing in Cardiology Challenge 2012 (Silva et al., 2012). The data reports 41 measurements of the first 48 hours of 8000 intensive care unit (ICU) patients. At a single time point an observation typically contains only a very small subset of measurements with measurements entirely missing for some patients.

### 4.2. Baselines

**Benchmarking on tabular data** We tested our method against four models that deal with irregularly sampled time series in a principled manner: (1) GRU-D (Che et al., 2018) uses trainable hidden state decay between observations and imputes missing values by a weighted average of previous observation and empirical mean. (2) ODE-RNN (Rubanova et al., 2019) alternates between continuous hidden state dynamics defined by an ODE and classical RNN updates at observation times. (3) Latent ODE (Chen et al. (2018), Rubanova et al. (2019)) is a generative model that uses ODE-RNN as recognition network to infer the initial value of its latent state and models the state evolution with an ODE. (4) GRU-ODE-Bayes (Brouwer et al., 2019) combines a continuous-time version of GRUs with a discrete update

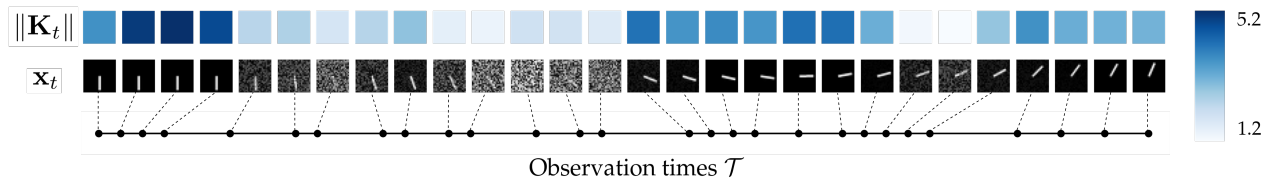


Figure 2. The figures shows noise corrupted observations and the corresponding Kalman gain norm for a pendulum trajectory sampled at irregular time intervals. The Kalman gain reflects the underlying noise process of the data.

network.

**Ablation study on image data** To assess the benefits of the continuity prior we used the pendulum image imputation set to compare our method against two RNNs with discrete state assumptions: GRUs (Cho et al., 2014a) and RKNs (Becker et al., 2019). For these models, we discretize the timeline in a preprocessing step. Precisely, we split the timeline into 20 equally spaced bins and keep the time point that is closest to the bin center. Note that methods mentioned in the previous paragraph have only been proposed for tabular data, which is why we do not consider them for the image prediction task.

#### 4.3. Qualitative analysis of the probabilistic state update

We are interested in how the probabilistic state space depicts uncertainty when updating the latent state. Two sources of uncertainty are considered: uncertainty arising from noise and from missing features.

**Noise robustness** We use the noise corrupted pendulum images to examine the gating mechanism of CRUs in the presence of high observation noise. Figure 2 shows how the norm of the Kalman gain mirrors the observation noise of a sample sequence. At times of high observation noise, the norm of the Kalman gain is small and consequently the gating mechanism acts in favor of the history encoded in the latent state prior. In contrast, when the pendulum is clearly observed, the Kalman gain attributes high weight to the new observation.

**Partial observability** To study the gating mechanism in the presence of partially observed inputs, we run the extrapolation task on the five-dimensional USHCN data while explicitly controlling the degree of partial observability. For each time point we sample one to four features each with probability 0.1. The remaining 60% of observations are fully observed to ensure stable learning. Figure 3 shows how the Kalman gain relates to the sparseness of an observation. The distribution of fully observed feature vectors (0% sparseness) is centered around comparably high values of the Kalman gain norm, whereas sparse observations are

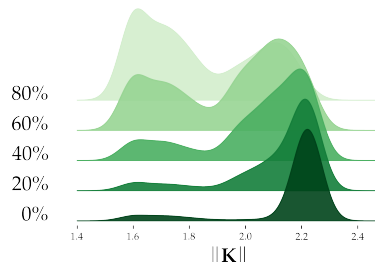


Figure 3. Distribution of the Kalman gain norm for different percentages of sparseness. For highly sparse observation vectors (e.g. 80% sparse), the distribution is shifted towards low norm values.

associated with lower Kalman gain norm values. Thus, the importance of the observation for the latent state update decreases with the observation’s sparseness.

#### 4.4. Results

We assess the performance of CRU against neural ODE and decay-based methods on interpolating and extrapolating the USHCN and Physionet data set. For extrapolation, we split the timeline into half and task the methods to predict the second half. In the interpolation task, models are evaluated on reconstructing the time series. We further test CRU against discrete RNNs on capturing dynamics of irregularly sampled pendulum images.

Table 1 reports mean squared error (MSE) and average runtime per epoch. The runtime measures a training pass through the entire dataset while keeping settings synchronized across architectures. CRU outperformed every other model on the interpolation task for both Physionet and USHCN data. Our method also produces the best extrapolation results on USHCN. On Physionet, latent ODE can better extrapolate patients trajectories than the autoregressive models considered. In contrast, autoregressive models seem to have an advantage on climatic data compared to the variational autoencoder (VAE)-based latent ODE model. This is plausible as the assumption of latent ODE - a trajectory determined by its initial value - is not fitting for dynamics chaotic as weather.

The efficient implementation variant, f-CRU, produces comparable results as the CRU baseline, while reducing training time by half. f-CRU outperforms neural ODE-method on both interpolation task and climate extrapolation. It is consistently the fastest method considered.

Table 1. Test MSE  $\times 10^{-2}$  (mean  $\pm$  std) and runtime (average seconds/epoch) on USHCN

Model	Interpolation	Extrapolation	Runtime
GRU-D	0.944 $\pm$ 0.011	1.718 $\pm$ 0.015	292
Latent ODE	1.798 $\pm$ 0.009	2.034 $\pm$ 0.005	110
ODE-RNN	0.831 $\pm$ 0.008	1.955 $\pm$ 0.466	81
GRU-ODE-B	0.841 $\pm$ 0.142	5.437 $\pm$ 1.020	389
f-CRU (ours)	<b>0.013 <math>\pm</math> 0.004</b>	1.569 $\pm$ 0.321	<b>61</b>
CRU (ours)	0.016 $\pm$ 0.006	<b>1.273 <math>\pm</math> 0.066</b>	122

Table 2. Test MSE  $\times 10^{-3}$  (mean  $\pm$  std) and runtime (average seconds/epoch) on Physionet. Where available, results are reported by Rubanova et al. (2019)

Model	Interpolation	Extrapolation	Runtime
GRU-D	3.384 $\pm$ 0.274	8.725 $\pm$ 0.713	5736
Latent ODE	2.118 $\pm$ 0.271	<b>2.231 <math>\pm</math> 0.029</b>	791
ODE-RNN	2.361 $\pm$ 0.086	4.668 $\pm$ 0.059	299
GRU-ODE-B	5.214 $\pm$ 0.384	7.980 $\pm$ 0.707	90
f-CRU (ours)	1.942 $\pm$ 0.068	8.772 $\pm$ 0.197	<b>62</b>
CRU (ours)	<b>1.818 <math>\pm</math> 0.912</b>	8.564 $\pm$ 0.607	114

To assess the benefits of continuous state transitions, we test our method against two RNN with discrete hidden state assumption: GRU and RKN. Methods are benchmarked on imputing missing images from irregularly sampled pendulum trajectories. Table 3 shows CRU outperforms both discrete RNNs by a large margin. The latter have difficulty capturing the dynamics once gaps between observations vary.

Table 3. Test MSE and Bernoulli NLL (mean  $\pm$  std) and runtime (average seconds/epoch) on Pendulum image prediction

Model	MSE ( $\times 10^{-3}$ )	Bernoulli NLL	Runtime
GRU	5.144 $\pm$ 0.057	23.169 $\pm$ 0.145	<b>11.6</b>
RKN	5.026 $\pm$ 0.092	22.720 $\pm$ 0.224	19.6
f-CRU (ours)	1.386 $\pm$ 0.162	15.519 $\pm$ 0.326	29.1
CRU (ours)	<b>0.996 <math>\pm</math> 0.052</b>	<b>14.405 <math>\pm</math> 0.110</b>	35.7

## 5. Conclusion

We presented CRU, a probabilistic neural network that models temporal data with non-uniform time intervals in a principled manner. We introduced the network architecture that incorporates a continuous version of the Kalman filter into an encoder-decoder structure thereby introducing a notion of uncertainty in the network’s gating mechanism. In an empirical study, we showed that the gating mechanism of CRU

weights noisy and partially observed input data concisely. We found that our method outperforms established recurrent structures such as GRU on irregular sampled image data and show that in comparison to neural ODE baselines, CRU achieved better results on interpolation.

## References

- Axelsson, P. and Gustafsson, F. Discrete-time solutions to the continuous-time differential lyapunov equation with applications to kalman filtering. *IEEE Transactions on Automatic Control*, 60(3):632–643, 2014.
- Becker, P., Pandya, H., Gebhardt, G., Zhao, C., Taylor, C. J., and Neumann, G. Recurrent kalman networks: Factorized inference in high-dimensional deep feature spaces. In *International Conference on Machine Learning*, pp. 544–552. PMLR, 2019.
- Brouwer, E. D., Simm, J., Arany, A., and Moreau, Y. Gru-ode-bayes: continuous modeling of sporadically-observed time series. In *Proceedings of the 33rd International Conference on Neural Information Processing Systems*, pp. 7379–7390, 2019.
- Cao, W., Wang, D., Li, J., Zhou, H., Li, L., and Li, Y. Brits: Bidirectional recurrent imputation for time series. *Advances in Neural Information Processing Systems*, 31: 6775–6785, 2018.
- Che, Z., Purushotham, S., Cho, K., Sontag, D., and Liu, Y. Recurrent neural networks for multivariate time series with missing values. *Scientific reports*, 8(1):1–12, 2018.
- Chen, R. T., Rubanova, Y., Bettencourt, J., and Duvenaud, D. Neural ordinary differential equations. In *Proceedings of the 32nd International Conference on Neural Information Processing Systems*, pp. 6572–6583, 2018.
- Cho, K., Van Merriënboer, B., Bahdanau, D., and Bengio, Y. On the properties of neural machine translation: Encoder-decoder approaches. *arXiv preprint arXiv:1409.1259*, 2014a.
- Cho, K., Van Merriënboer, B., Gulcehre, C., Bahdanau, D., Bougares, F., Schwenk, H., and Bengio, Y. Learning phrase representations using rnn encoder-decoder for statistical machine translation. *arXiv preprint arXiv:1406.1078*, 2014b.
- Choi, E., Xiao, C., Stewart, W. F., and Sun, J. Mime: Multi-level medical embedding of electronic health records for predictive healthcare. *arXiv preprint arXiv:1810.09593*, 2018.
- Chung, J., Kastner, K., Dinh, L., Goel, K., Courville, A. C., and Bengio, Y. A recurrent latent variable model for se-

- quential data. *Advances in neural information processing systems*, 28:2980–2988, 2015.
- Fraccaro, M., Kamronn, S. D., Paquet, U., and Winther, O. A disentangled recognition and nonlinear dynamics model for unsupervised learning. In *31st Conference on Neural Information Processing Systems*, 2017.
- Herrera, C., Krach, F., and Teichmann, J. Neural jump ordinary differential equations: Consistent continuous-time prediction and filtering. In *International Conference on Learning Representations*, 2020.
- Hochreiter, S. and Schmidhuber, J. Long short-term memory. *Neural computation*, 9(8):1735–1780, 1997.
- Jazwinski, A. H. *Stochastic Processes and Filtering Theory*. Academic Press, 1970.
- Kalman, R. E. A new approach to linear filtering and prediction problems. 1960.
- Karl, M., Soelch, M., Bayer, J., and Van der Smagt, P. Deep variational bayes filters: Unsupervised learning of state space models from raw data. *arXiv preprint arXiv:1605.06432*, 2016.
- Kidger, P., Morrill, J., Foster, J., and Lyons, T. Neural controlled differential equations for irregular time series. *arXiv preprint arXiv:2005.08926*, 2020.
- Krishnan, R. G., Shalit, U., and Sontag, D. Deep kalman filters. *arXiv preprint arXiv:1511.05121*, 2015.
- Lechner, M. and Hasani, R. Learning long-term dependencies in irregularly-sampled time series. *Advances in Neural Information Processing Systems*, 33, 2020.
- Lezcano-Casado, M. Trivializations for gradient-based optimization on manifolds. In *Advances in Neural Information Processing Systems, NeurIPS*, pp. 9154–9164, 2019.
- Lipton, Z. C., Kale, D., and Wetzel, R. Directly modeling missing data in sequences with rnns: Improved classification of clinical time series. In *Machine learning for healthcare conference*, pp. 253–270. PMLR, 2016.
- Menne, M., Williams Jr, C., and Vose, R. Long-term daily climate records from stations across the contiguous united states, 2015.
- Morrill, J., Salvi, C., Kidger, P., and Foster, J. Neural rough differential equations for long time series. In *International Conference on Machine Learning*, pp. 7829–7838. PMLR, 2021.
- Mozer, M. C., Kazakov, D., and Lindsey, R. V. Discrete event, continuous time rnns. *arXiv preprint arXiv:1710.04110*, 2017.
- Rome, H. A direct solution to the linear variance equation of a time-invariant linear system. *IEEE Transactions on Automatic Control*, 14(5):592–593, 1969.
- Rubanova, Y., Chen, R. T., and Duvenaud, D. Latent odes for irregularly-sampled time series. In *Proceedings of the 33rd International Conference on Neural Information Processing Systems*, pp. 5320–5330, 2019.
- Shukla, S. N. and Marlin, B. M. A survey on principles, models and methods for learning from irregularly sampled time series. *arXiv preprint arXiv:2012.00168*, 2020.
- Silva, I., Moody, G., Scott, D. J., Celi, L. A., and Mark, R. G. Predicting in-hospital mortality of icu patients: The physionet/computing in cardiology challenge 2012. In *2012 Computing in Cardiology*, pp. 245–248. IEEE, 2012.

## 6. Appendix

### 6.1. Efficient prior computation

For an efficient implementation, we assume locally linear transitions with symmetric basis matrices  $\{\mathbf{A}^{(k)}\}_{k=1\dots K}$  that share the same eigenvectors.

$$\mathbf{A}_t = \sum_{k=1}^K \alpha_t^{(k)} \mathbf{A}^{(k)} \quad \text{with} \quad \mathbf{A}^{(k)} = \mathbf{E} \mathbf{D}^{(k)} \mathbf{E}^T \quad (20)$$

#### 6.1.1. PRIOR MEAN

We can simplify the matrix exponential in Equation (7) to the elementwise exponential function. The exponential of a diagonalizable matrix can be obtained by exponentiating each entry on the main diagonal of eigenvalues:

$$\begin{aligned} \boldsymbol{\mu}_{t'}^- &= \exp\left(\mathbf{A}_t(t' - t)\right) \boldsymbol{\mu}_t^+ \\ &= \exp\left(\sum_{k=1}^K \alpha^{(k)} \mathbf{A}^{(k)}(t' - t)\right) \boldsymbol{\mu}_t^+ \\ &= \exp\left(\sum_{k=1}^K \alpha^{(k)} \mathbf{E} \mathbf{D}^{(k)} \mathbf{E}^T(t' - t)\right) \boldsymbol{\mu}_t^+ \\ &= \mathbf{E} \exp\left(\sum_{i=1}^K \alpha^{(k)} \mathbf{D}^{(k)}(t' - t)\right) \mathbf{E}^T \boldsymbol{\mu}_t^+ \end{aligned} \quad (21)$$

#### 6.1.2. PRIOR COVARIANCE

For diagonalizable transition matrices of a linear time-invariant system Rome (1969) proposes an analytical solution for the computation of the prior covariance based on



the eigendecomposition of the transition matrix. Precisely, we can define a new state vector  $\mathbf{w}$  with covariance  $\Sigma_t^w$

$$\mathbf{w}_t = \mathbf{E}^T \mathbf{z}_t \quad \Sigma_t^w = \mathbf{E}^T \Sigma_t^+ \mathbf{E} \quad (22)$$

We further define  $\tilde{\mathbf{D}}$  as the matrix whose  $ij$ -th element is the sum of the  $i$ -th and  $j$ -th diagonal entry of  $\sum_{k=1}^K \mathbf{D}^{(k)}$  i.e.  $\tilde{\mathbf{D}}_{ij} = \sum_{k=1}^K \mathbf{D}_{ii}^{(k)} + \mathbf{D}_{jj}^{(k)}$ . Let  $\mathbf{S} = \mathbf{E}^T \mathbf{G} \mathbf{Q} \mathbf{G}^T \mathbf{E}$  then we can compute the covariance of  $\mathbf{w}$  at time  $t'$  with

$$\Sigma_{t'}^w = (\mathbf{S} \odot e^{\tilde{\mathbf{D}}(t'-t)} - \mathbf{S}) \odot \tilde{\mathbf{D}} + \Sigma_t^w \odot e^{\tilde{\mathbf{D}}(t'-t)} \quad (23)$$

Mapping back to the space of  $\mathbf{z}$  we obtain for the prior covariance of  $\mathbf{z}$  at time  $t'$

$$\Sigma_{t'}^- = \mathbf{E} \Sigma_{t'}^w \mathbf{E}^T \quad (24)$$

## 6.2. Matrix fraction decomposition

The integral in the prior covariance (Equation (8)) can be resolved analytically using matrix fraction decomposition (Axelsson & Gustafsson, 2014). The method is based on taking the matrix exponential of the matrix  $\mathbf{B}$

$$\mathbf{B} = \begin{pmatrix} \mathbf{A} & \mathbf{G} \mathbf{Q} \mathbf{G}^T \\ \mathbf{0} & -\mathbf{A}^T \end{pmatrix} \quad \exp(\mathbf{B}(t'-t)) = \begin{pmatrix} \mathbf{M}_1 & \mathbf{M}_2 \\ \mathbf{0} & \mathbf{M}_3 \end{pmatrix} \quad (25)$$

The prior covariance matrix is then given by

$$\Sigma_{t'}^- = \exp(\mathbf{A}(t'-t)) \Sigma_t^+ \exp(\mathbf{A}(t'-t))^T + \mathbf{M}_2 \exp(\mathbf{A}(t'-t))^T \quad (26)$$

## 6.3. Approximations

In their work on RKNs Becker et al. (2019) exploit assumptions on the structure of components of the Kalman filter to simplify computation. In particular, they reduce the matrix inversion in the Kalman gain to elementwise operations. We also exploit these approximations in the Kalman cell of CRU.

**Observation model** The dimension of the latent state  $M$  is twice of the dimension of the latent observation space  $D$ , i.e.  $M = 2D$ . The observation model links both spaces and is fixed at  $\mathbf{H} = [\mathbf{I}_D, \mathbf{0}_D]$  where  $\mathbf{I}_D$  denotes the  $D$ -dimensional identity matrix and  $\mathbf{0}_D$  the  $D$ -dimensional zero matrix. The idea is to split the latent state into an *observed part* that extracts information directly from the observations and a *memory part* that encodes features inferred over time.

**State covariance** The covariance matrix of the latent state  $\Sigma_t$  is built of diagonal blocks  $\Sigma_t^u, \Sigma_t^l, \Sigma_t^s$  whose vectors of diagonal entries are denoted by  $\sigma_t^u, \sigma_t^l, \sigma_t^s$  respectively.

$$\Sigma_t = \begin{pmatrix} \Sigma_t^u & \Sigma_t^s \\ \Sigma_t^s & \Sigma_t^l \end{pmatrix} \quad (27)$$

The observation part of the latent state is thus only correlated with the corresponding memory part. The argument behind this strong assumption is that the free parameters in the neural encoder and decoder suffice to find a representation where above limitations hold.

**Simplified update step** The Kalman gain simplifies to a structure with two diagonal blocks of size  $D \times D$ , i.e.  $\mathbf{K}_t = [\mathbf{K}_t^u \quad \mathbf{K}_t^l]^T$ . The vector of diagonal entries  $\mathbf{k}_t^u, \mathbf{k}_t^l$  can be computed with element wise division ( $\odot$ )

$$\mathbf{k}_t^u = \sigma_t^{u,-} \odot (\sigma_t^{u,-} + \sigma_t^{\text{obs}}) \quad \mathbf{k}_t^l = \sigma_t^{s,-} \odot (\sigma_t^{u,-} + \sigma_t^{\text{obs}}) \quad (28)$$

The posterior mean update then simplifies to

$$\mu_t^+ = \mu_t^- + \begin{bmatrix} \mathbf{k}_t^u \\ \mathbf{k}_t^l \end{bmatrix} \odot \begin{bmatrix} \mathbf{y}_t - \mu_t^{u,-} \\ \mathbf{y}_t - \mu_t^{u,-} \end{bmatrix} \quad (29)$$

where  $\mu_t^u$  and  $\mu_t^l$  denote the upper and lower part of the prior mean respectively i.e.  $\mu_t^- = [\mu_t^{u,-} \quad \mu_t^{l,-}]^T$ . The update of the posterior covariance reduces to

$$\sigma_t^{u,+} = (\mathbf{1}_m - \mathbf{k}_t^u) \odot \sigma_t^{u,-} \quad (30)$$

$$\sigma_t^{s,+} = (\mathbf{1}_m - \mathbf{k}_t^u) \odot \sigma_t^{s,-} \quad (31)$$

$$\sigma_t^{l,+} = \sigma_t^{l,-} - \mathbf{k}_t^l \odot \sigma_t^{s,-} \quad (32)$$

where  $\odot$  denotes elementwise multiplication.

## 6.4. Implementation details

For all experiments we used a transition net with one linear layer and softmax output. The encoders for all experiments have a linear output layer for the latent observation and a separate linear output layer with experiment-specific activation function for the latent observation variance.

### 6.4.1. PENDULUM STATE ESTIMATION

We used a latent observation dimension of 15 and a latent state dimension of 30. The transition model is locally linear with 15 basis matrices of bandwidth 3.

**Encoder:** 2 convolution, 1 fully connected, linear output

1. Layer: Convolution, 12 channels,  $5 \times 5$  kernel, padding 2, ReLU, max pooling with  $2 \times 2$  kernel and  $2 \times 2$  stride
2. Layer: Convolution, 12 channels,  $3 \times 3$  kernel, padding 1,  $2 \times 2$  stride, ReLU, max pooling with  $2 \times 2$  kernel and  $2 \times 2$  stride
3. Layer: Fully-connected, 30 neurons, ReLU
4. Layer: latent observation: linear output; latent observation variance: linear output, elu+1 activation

**Decoder o:** 1 fully-connected, linear output

1. Layer: Fully connected, 30 neurons, Tanh
2. Layer: Linear output

**Decoder  $\sigma^{\text{out}}$ :** 1 fully-connected, linear output

1. Layer: Fully connected, 30 neurons, Tanh
2. Layer: Linear output, elu+1 activation

#### 6.4.2. PENDULUM IMAGE IMPUTATION

We used the same encoder, latent dimensions and transition model as in the pendulum state estimation task.

**Decoder o:** 1 fully-connected, 3 transposed convolution

1. Layer: Fully connected, 144 neurons, ReLU
2. Layer: Transposed Convolution, 16 channels,  $5 \times 5$  kernel, padding 2,  $4 \times 4$  stride, ReLU
3. Layer: Transposed Convolution, 12 channels,  $3 \times 3$  kernel, padding 1,  $2 \times 2$  stride, ReLU
4. Layer: Transposed Convolution, 1 channel,  $2 \times 2$  kernel, padding 5,  $2 \times 2$  stride, Sigmoid

#### 6.4.3. USHCN

We chose the same dimensionality for the latent observation as the data and a latent state of 10 dimensions. The transition model consists of 15 basis matrices of bandwidth 3.

**Encoder:** 3 fully connected, linear output

1. Layer: Fully connected, 50 neurons, ReLU, layer normalization

2. Layer: Fully connected, 50 neurons, ReLU, layer normalization

3. Layer: Fully connected, 50 neurons, ReLU, layer normalization

4. Layer: latent observation: linear output; latent observation variance: linear output, squared activation

**Decoder o:** 3 fully connected, linear output

1. Layer: Fully connected, 50 neurons, ReLU, layer normalization

2. Layer: Fully connected, 50 neurons, ReLU, layer normalization

3. Layer: Fully connected, 50 neurons, ReLU, layer normalization

4. Layer: latent observation: linear output; latent observation variance: linear output, squared activation

**Decoder  $\sigma^{\text{out}}$ :** 1 fully-connected, linear output

1. Layer: Fully connected, 50 neurons, ReLU, layer normalization

2. Layer: Linear output, squared activation

#### 6.4.4. PHYSIONET

We used 10 dimensions for the latent observation and 20 for the latent state. We chose 20 fully parameterized basis matrices. The encoder and decoder architecture is the same as in the USHCN experiment.

### 6.5. Training details

We trained CRU with Adam optimizer () and learning rate 0.001. We found a slightly higher learning rate of 0.005 to work best for CRU-eig. For scalar data sets, we used gradient clipping. We trained until convergence for 100 epochs. We used a batchsize of 50 for climate and pendulum data and a batchsize of 100 for Physionet.

The initial conditions for the latent state are  $\mu_{t_0}^- = \mathbf{0}$  and  $\Sigma_{t_0}^- = 10 \cdot \mathbf{I}$ . We found an initialization of the transitions such that the prior mean is close to the posterior mean of the previous time step crucial for performance and stability. Thus, we initialized the basis matrices  $\{\mathbf{A}^{(k)}\}_{k=1\dots K}$  filled with zeros to start off with a prediction step of  $\mu_t^- = \mathbf{I}\mu_t^+$ . Equivalently, we chose  $\mathbf{E} = \mathbf{I}$  and  $\mathbf{D}^{(k)} = 1e^{-5} \cdot \mathbf{I}$ ,  $k = 1\dots K$  for the CRU-eig variant.

## 6.6. Data preprocessing

**USHCN** Daily weather records can be downloaded at [https://cdiac.ess-dive.lbl.gov/ftp/ushcn\\_daily/](https://cdiac.ess-dive.lbl.gov/ftp/ushcn_daily/). We remove observations with a bad quality flag and select a four years time window from 1990 to 1993. We keep only centers that start reporting before 1990 and end reporting after 1993. We split the remaining 1168 centers into 60% train 20% validation and 20% test set. For each set, we remove measurements that are more than four standard deviations away from the set mean and normalize each feature to be in [0,1] interval individually per set. For applying CRU, we scale the timestamps, which unit is days, by a factor of 0.3.

**Physionet** The data is publicly available for download at <https://physionet.org/content/challenge-2012/1.0.0/>. We discard four general descriptors reported once at admission (age, gender, height, ICU-type) and keep only the remaining set of 37 time-variant features. We split the patients into 60% train, 20% validation and 20% test set. Lastly, we normalize each feature to be in [0,1] interval separately per set.